ISSN 2070-2051, Protection of Metals and Physical Chemistry of Surfaces, 2016, Vol. 52, No. 4, pp. 704–713. © Pleiades Publishing, Ltd., 2016.

PHYSICOCHEMICAL PROBLEMS OF MATERIALS PROTECTION

Protection of 6061 Al-15%$_{(v)}$ SiC$_{(P)}$ Composite from Corrosion by a Biopolymer and Surface Morphology Studies[1]

B. P. Charitha and Padmalatha Rao*

Chemistry department, Manipal Institute of Technology, Manipal, India

**e-mail: padmalatha.rao@manipal.edu*

Received November 21, 2015

Abstract—The protective action of biopolymer starch on 6061 Al-15%$_{(v)}$ SiC $_{(P)}$ composite in 0.25 M hydrochloric acid was studied by potentiodynamic polarization (PDP) and electrochemical impedance spectroscopy (EIS) techniques with temperature ranging from 303 to 323 K. The concentrations of starch used were in the range of 0.1 to 0.8 g L^{-1}. The surface morphology studies were carried out using Scanning Electron Microscope, Energy Dispersive X-ray analysis, Atomic Force Microscope and X-ray Diffraction analysis techniques. Suitable mechanism was proposed for the corrosion and inhibition process. Results indicated increase in the efficiency of the inhibitor with its increase in the concentration and with temperature. Maximum inhibition efficiency of 84% was observed at 323 K for 0.8 g L^{-1}. Starch acted as a mixed inhibitor. Kinetic and thermodynamic studies showed that starch underwent chemical adsorption and obeyed Langmuir adsorption isotherm. Surface morphology studies confirmed the adsorption of inhibitor on the surface of metal matrix composite. Results obtained by potentiodynamic polarization method and electrochemical impedance spectroscopy method were in good agreement with one another.

DOI: 10.1134/S2070205116040079

INTRODUCTION

Aluminum alloys reinforced with nanostructured SiC particulates are called as Aluminum Metal Matrix Composites (AlMMC's). Compared to the base alloys, the reinforced composites have high specific strength, damping capacity, specific modulus and good wear resistance. They have wide range of application in aerospace, automotive etc. [1]. Reinforcement of the alloy makes it vulnerable for corrosion attack. This is mainly because of difference in potential of matrix and the reinforced material. During surface treatment of these composites by pickling process mineral acids not only removes the extraneous matter deposited on the metal surface, but also results in considerable material loss due to corrosion [2]. The addition of corrosion inhibitors to the corrosive is one of the alternatives to reduce the rate of corrosion attack. Most commonly chemical compounds are used as corrosion inhibitors, but due to environmental regulation use of chemical inhibitors are restricted.

Biopolymers are one of the classes of ecofriendly inhibitors, which are naturally available, cheap, nontoxic, environmentally friendly and biodegradable. The biopolymer of present study is starch which has wide range of applications in food industry, paper making, pharmaceuticals and many other industrial branches [3].

As a part of studies with ecofriendly inhibitors [4–6], for corrosion control of aluminum, aluminum alloys and composite materials, we report herein the applicability of biopolymer starch to control the corrosion aluminum composite in hydrochloric acid medium.

EXPERIMENTAL

Material: 6061 Al-15%$_{(V)}$ SiC$_{(P)}$ composite was used to perform the experiment. Base alloy composition is given in the table1.

Preparation of test coupon: Aluminum composite metal of 1cm^2 surface area sealed with resin material was exposed to HCl medium. Polishing was carried out using different graded emery papers. Then disc polishing was done using levigated alumina in order to get the mirror surface; the freshly polished specimen was dried and kept in the desiccators for further studies.

Preparation of inhibitor solution: Starch (Merck chemicals) was used as such. The inhibitor stock solution was prepared by dissolving starch (1 g) in boiling water and made up to 1 L with hydrochloric acid.

Table 1. The composition of the base metal 6061 Al- alloy

Elements	Cu	Mg	Cr	Si	Al
Composition (wt %)	0.02	0.61	0.01	1.00	Balance

[1] The article is published in the original.

Electrochemical studies: With the help of Potentiostat (CH600 D-series, U.S. model with CH-instrument beta software) the electrochemical studies were carried out using 6061 Al-15%$_{(V)}$ SiC$_{(P)}$ composite material, Saturated Calomel electrode and Pt-electrode.

The potentiodynamic polarization studies were performed by allowing the metal to attain steady state open circuit potential in 0.25 M HCl medium for 1800 s. It was then polarized from −250 mV cathodically to +250 mV anodically with respect to OCP at a sweep rate of 1mV s^{-1}.

The EIS studies were performed by applying small amplitude of AC signal of 10 mV at the OCP with a frequency range from 10 000 Hz to 0.01 Hz. The analysis of impedance data was done by using Nyquist plot. 3 to 4 trials were carried out and best of the three agreeing values were reported.

Surface morphology studies: Surface morphology studies and elemental analysis were done using analytical scanning electron microscope and Energy Dispersive X-Ray analysis respectively. AFM analysis was performed by using 1B342 innova model. All the studies were carried out by immersing the metal for 2 h in the acid medium and medium containing inhibitor. XRD analysis was done for the scraped products of aluminum composite obtained by immersing the metal in 0.25 M HCl and in inhibited solution.

RESULTS AND DISCUSSION

Fourier transforms infrared (FTIR) spectroscopy of starch. Figure 1 is the FTIR spectrum for starch. The region between 900 and 1500 cm^{-1} is the fingerprint region, the absorption bands at 979, 1087, 1164, 1257, 1365, 1465 cm^{-1} is attributed to –C–O–C–, 1650 cm^{-1} peak is for tightly bounded H_2O present in starch and 3541 and 3101 cm^{-1} absorption bands are due to characteristic vibrations of C–H and –OH bonds respectively.

Potentiodynamic polarization (PDP) measurement: Plots of potentiodynamic polarization studies for the corrosion of 6061 Al-15%$_{(v)}$ SiC$_{(P)}$ composite in 0.25 M HCl solution containing various concentrations of starch are shown in Fig. 2. Corresponding results are tabulated in Table 2.

Potentiodynamic polarization plots indicates active dissolution of 6061 Al-15%$_{(v)}$ SiC$_{(P)}$ composite in acidic environment. Anticorrosive capacity of starch is also very much evident from the tabulated values.

Various parameters such as corrosion potential (E_{corr}), corrosion current density (i_{corr}), cathodic Tafel slopes (-β_c) anodic Tafel slopes (-β_a) values were obtained by potentiodynamic polarization studies. By using i_{corr} values percentage inhibition efficiency [I.E(%)] of inhibitor was calculated by using Eq. (1) [14].

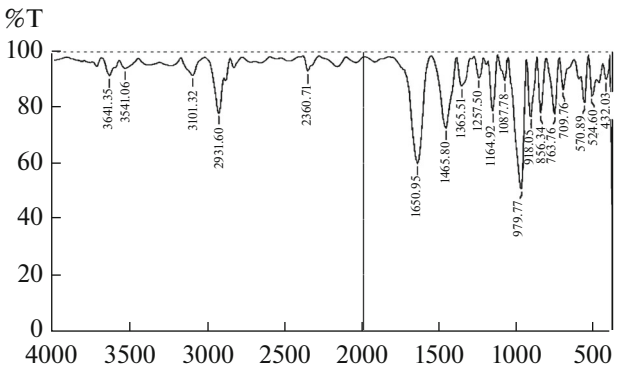

Fig. 1. FTIR spectrum of starch.

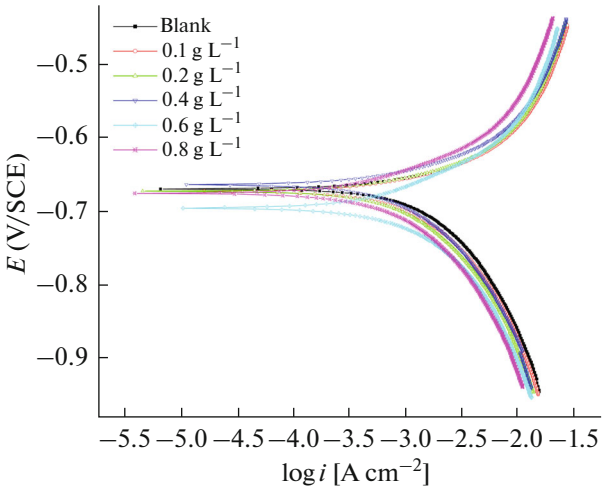

Fig. 2. Potentiodynamic polarization plots in 0.25 M hydrochloric acid containing different concentrations of starch at 308K of 6061Al-15%$_{(V)}$ SiC$_{(P)}$.

$$\text{I.E.}(\%) = \frac{i_{corr} - i_{corr(inh)}}{i_{corr}} \times 100. \quad (1)$$

Then the corrosion rate in mmy^{-1} was obtained by using the Eq. (2)

$$\text{CR (mmy}^{-1}) = \frac{3270 \times M \times i_{corr}}{\rho \times z}, \quad (2)$$

where, 3270 is a constant which revels the unit of corrosion rate, ρ is corroding material density of aluminum composite i.e. 2.66 g cm^{-3}, M is the atomic mass of aluminum composite (9.15), Z is the electrons transferred per metal atom (3) [15].

Since the plateau of anodic current is not well defined the corrosion current density were determined by extrapolation of cathodic slopes. Further, there was no remarkable change in the value of cathodic Tafel slopes after the addition of inhibitor. This suggests the blocking effect of inhibitor on the surface of the metal.

Table 2. Results of potentiodynamic polarization measurements in 0.25 M hydrochloric acid containing different concentrations of starch at different temperatures for the corrosion of 6061 Aluminum $15\%_{(V)}$ $SiC_{(P)}$

Temp (K)	[Starch], g L^{-1}	E_{corr}, mV/ SCE	i_{corr}, mA cm^{-2}	$-\beta_c$, mV dec^{-1}	CR, mmy^{-1}	I.E., %
303	Blank	—669	19.0	563	7.2	–
	0.1	—677	15.0	572	5.68	21.09
	0.2	—672	12.5	605	5.55	33.92
	0.4	—669	11.4	589	4.98	39.48
	0.6	—671	10.6	589	3.49	44.56
	0.8	—670	10.1	593	2.76	46.74
308	Blank	—669	22.0	549	9.83	–
	0.1	—679	16.7	585	7.31	24.12
	0.2	—672	15.2	564	6.43	30.59
	0.4	—663	13.3	593	5.02	39.57
	0.6	—693	10.7	576	4.13	51.24
	0.8	—670	10.4	600	3.29	52.33
313	Blank	—669	24.5	563	12.11	–
	0.1	—672	16.9	583	8.29	31.13
	0.2	—672	15.3	605	6.77	37.65
	0.4	—671	13.0	589	5.64	46.69
	0.6	—670	10.1	574	4.61	58.47
	0.8	—752	9.98	600	3.59	59.33
318	Blank	—675	36.0	513	17.29	–
	0.1	—673	21.2	581	8.99	41.12
	0.2	—669	18.9	564	7.43	47.33
	0.4	—669	15.6	563	6.51	56.54
	0.6	—652	11.3	596	5.06	68.64
	0.8	—676	11.0	612	3.69	69.36
323	Blank	—683	44.5	597	22.78	–
	0.1	—677	19.7	665	16.61	55.63
	0.2	—695	16.7	644	8.45	62.53
	0.4	—695	12.8	785	7.10	71.22
	0.6	—677	7.69	775	5.58	82.75
	0.8	—652	7.38	701	3.84	83.44

The added inhibitor results in surface inactivation and do not alter the mechanism of corrosion process.

Higher corrosion rate of aluminum composite is mainly because of the presence of reinforcing element SiC. Electrode potential of Si is –0.14 V and electrode potential of Al is –1.67 V. Thus SiC particulates acts as cathodic site with aluminum matrix as anode. This sets in galvanic corrosion leading to the disintegration of aluminum matrix. Due to the heterogeneous nature and the presence of SiC particulate matter in composite material active sites for the adsorption of inhibitor become more.

Corrosion potential (E_{corr}) did not change remarkably after the addition of inhibitor [16]. As per the reported literature, if the shift in E_{corr} exceeds ±85 mV in comparison with uninhibited solutions, the inhibitor behaves distinctly as either cathodic or anodic inhibitor. In the present investigation, displacement of E_{corr} is not more than +30 mV and it is more towards positive direction [17]. This observation indicates that starch may act as mixed inhibitor and inhibits anodic reaction of aluminum composite material corrosion. Starch, as it is a larger molecule it may control the corrosion process by forming a protective film on both

anodic and cathodic area, thus behaves as mixed inhibitor.

The maximum inhibition efficiency was found to be 83.44% for 6061 Al-15%$_{(V)}$ SiC$_{(P)}$ composite 0.25 M HCl at 323 K for inhibitor concentration of 0.8 g L^{-1}.

Electrochemical Impedance Spectroscopy (EIS) studies: Nyquist plots of 6061 Al-15%$_{(V)}$ SiC$_{(P)}$ composite for uninhibited and inhibited medium in 0.25 M HCl medium are shown in the Fig. 3.

Semicircle impedance plots were obtained for both 6061Al-15%$_{(V)}$ SiC$_{(P)}$ in uninhibited and inhibited medium containing 0.25 M hydrochloric acid. Impedance plots of same type have been reported in the literature for the corrosion control of Al and its alloys in HCl medium [11, 12].

Oxidation of 6061 Al-15 vol % SiC$_{(P)}$ at M^+/oxide/solution interface corresponds to HF capacitive loop. During the process of corrosion, Al^{+1} will get oxidized to Al^{+3}. The oxidation of Al^{+3} is due to the migration of Al^{+1} from M^+/oxide interface through oxide/electrolyte interface. At oxide/solution interface OH^- and O^{2-} ions are formed. The Figure 3 showing single capacitive loop indicates that it is undergoing all the three process this is either due to domination of one process over the other or due to the overlapping of loops during the corrosion process, and also capacitive loop in high frequency region is attributed for the formation of passivating oxide film onto the surface of the metal [13]. As the inhibitor concentration increased, the capacitive loop diameter increased, this indicates resistance to corrosion attack by the adsorption of inhibitor molecule [14]. Inductive loop at LF is formed because of the relaxation of bulk or surface species in the protective oxide film and it may also due to the adsorbed inhibitor molecule relaxation over the aluminum surface or due to Cl^- ions incorporation, charged intermediates and O^{2-} ions on and into the protective layer of oxide. Due to the electrode surface inhomogeneity, the semicircles of the Nyquist plots were depressed [15].

Figure 4a is the five element equivalent circuit which was used to simulate the impedance plots for 6061Al-15%$_{(V)}$ SiC$_{(P)}$.

The equivalent circuit consists of five elements; they are Solution resistance (R_S), Charge transfer resistance (R_{ct}), Inductive resistance (R_L) and inductive element (L). It also consist of CPE (Constant Phase Element, Q), which is parallel to resistors and inductive element shown in the Fig. 4a. Due to the presence of inductive loop the R_P value can be calculated by using Eq. (3),

$$R_P = \frac{R_L R_{ct}}{R_L R_{ct}}. \quad (3)$$

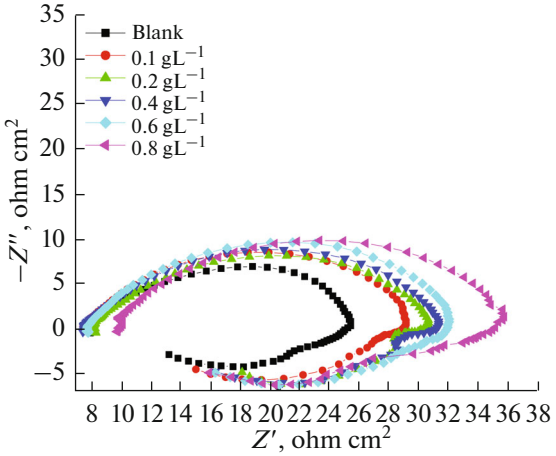

Fig. 3. Nyquist plots in 0.25 M hydrochloric acid containing different concentrations of starch at 308 K of 6061 Al-15%$_{(V)}$ SiC$_{(P)}$.

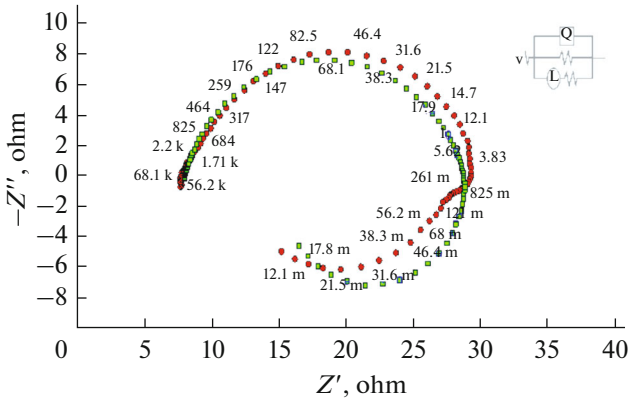

Fig. 4. a—Equivalent circuit used to simulate for the obtained impedance values. b—Impedance data obtained for 6061Al-15%$_{(V)}$ SiC$_{(P)}$ corrosion in 0.25M HCl at 308K.

Nyquist plots are depressed. Thus, in the circuit fitment, the component Q_{dl}, and coefficient "a" of Q(CPE) quantifies some physical phenomena like inhomogeneous of surface of the metal, binding of the inhibitor molecule and formation of porous layer etc. [16]

$$C_{dl} = Q_{dl}(2\pi f_{max})^{(a-1)} \quad (4)$$

As polarization resistance (R_P) are inversely related to the corrosion current density (i_{corr}). The percentage I.E. can be obtained by using the Eq. (5)

$$\text{I.E.}(\%) = \frac{R_{P(inh)} - R_P}{R_{P(inh)}} \times 100. \quad (5)$$

R_P and $R_{P(inh)}$ are the polarization resistance for blank and in the presence of the inhibitor. R_P value obtained from Potentiodynamic polarization measurement is in good agreement with R_P value obtained

Table 3. Results of EIS measurements in 0.25 M hydrochloric acid containing different concentrations of Starch at different temperature for the corrosion of 6061Al-15%$_{(V)}$ SiC$_{(P)}$

Temp., K	[Starch], g L^{-1}	C_{dl}, $\times 10^2$ μF	R_p, Ω cm^2	I.E., %
303	Blank	338.5	6.09	–
	0.1	323.1	8.10	21.09
	0.2	312.7	8.96	33.92
	0.4	301.0	10.01	39.48
	0.6	296.8	11.05	44.56
	0.8	289.7	11.75	46.74
308	Blank	359.5	5.94	–
	0.1	341.4	8.04	24.12
	0.2	336.1	8.65	30.59
	0.4	328.0	9.75	39.57
	0.6	317.4	11.65	51.24
	0.8	306.5	12.86	52.33
313	Blank	433.9	5.31	–
	0.1	424.0	7.74	31.13
	0.2	415.1	8.16	37.65
	0.4	409.3	9.48	46.69
	0.6	386.0	11.56	58.47
	0.8	352.3	12.50	59.33
318	Blank	444.2	3.53	–
	0.1	423.4	5.94	41.12
	0.2	417.8	6.53	47.33
	0.4	399.9	7.92	56.54
	0.6	368.2	10.97	68.64
	0.8	341.4	11.06	69.36
323	Blank	467.5	2.51	–
	0.1	442.5	5.92	55.63
	0.2	436.0	6.50	62.53
	0.4	421.3	7.89	71.22
	0.6	415.2	10.96	82.75
	0.8	386.4	11.17	83.44

from Electrochemical Impedance Spectroscopy studies indicates that rate of corrosion does not depends upon the technique used but it depends upon the inhibitor behavior [17].

Table 3 revels that R_P values were increased with enhancing the concentration of inhibitor but CPE value decreased this is because of increased thickness of electrical double layer at M^+/solution interface [18]. At the interface of charged metal surface and the solution, there will be formation of electrical double layer. This electrical double layer is equivalent to an electrical capacitor. Usually, as a result of adsorption of the inhibitors on the metal surface, capacitance of electrical double layer (C_{dl}) decreases. This is because of adsorption of inhibitor molecules takes place by the displacement of water molecules and other ions originally adsorbed on the metal surface. Capacitance of electrical double layer (C_{dl}) is related to thickness of the double layer (d) and the local dielectric constant (ε) by following equation (6)

$$C_{dl} = \varepsilon/4\pi d. \quad (6)$$

Effect of temperature: It is evidence from the Table 2 that, I.E (%) of the starch inhibitor increased with increase in the temperature. This increase in I.E (%) is due to the firm adsorption of the adsorbed inhibitor molecule onto the surface of the metal [19]. Kinetic parameters such as energy of activation (E_a), the enthalpy (ΔH_a) and entropy of activation (ΔS_a) values can be obtained by studying the effect of temperature on the adsorption of inhibitor over the surface of the metal. The energy of activation (E_a) can be calculated from Arrhenius law equation [20],

$$\ln(\mathrm{CR}) = B - \frac{E_a}{RT}, \quad (7)$$

where, B is Arrhenius constant which depends upon the metal type and R is equal to 8.314 J K^{-1} mol^{-1} (universal gas constant), T is the absolute temperature. Figure 5 is the Arrhenius plots for the Al-composite material in various concentration of starch inhibitor in 0.25 M hydrochloric acid. The plots of ln (CR) verses $1/T$ gave collinear lines with a slope corresponding to $-E_a/R$ from which energy of activation (E_a) values was obtained for the aluminum composite corrosion and its inhibition process.

The transition state equation was used to calculate the enthalpy (ΔH_a) and entropy of activation (ΔS_a) for the dissolution of metal. The transition state equation is [21],

$$CR = \frac{RT}{Nh}\exp\left(\frac{\Delta S_a}{R}\right)\exp\left(-\frac{\Delta H_a}{RT}\right), \quad (8)$$

where h is planks constant (6.626×10^{-34} J s), N is Avogadro's number (6.023×10^{23} mol^{-1}). The plot of ln (CR/T) verses $1/T$ gave a collinear line with slope corresponding to $-\frac{\Delta H_a}{R}$, which gave the value of enthalpy of activation and the intercept corresponding to $\ln(\mathrm{R/Nh}) + \frac{\Delta S_a}{R}$ gave the value of entropy of activation. Figure 6 is the plot of ln (CR/T) verses $1/T$ for Al-composite in various concentration of starch inhibitor in 0.25 M hydrochloric acid. Activation parameters for the corrosion of aluminum and Al-composite in 0.25 M hydrochloric acid containing different concentrations of starch inhibitors are tabulated in Table 4.

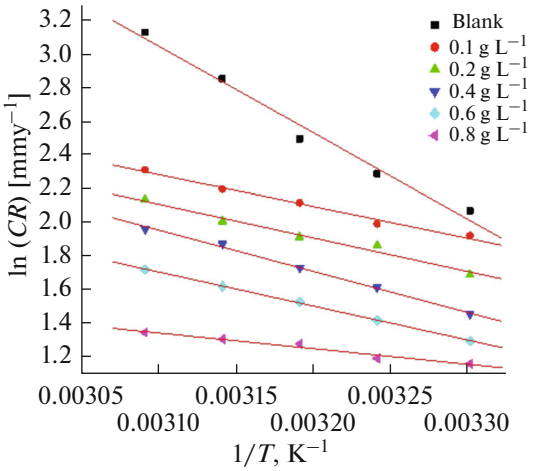

Fig. 5. Arrhenius plots in 0.25 M hydrochloric acid containing different concentrations of starch for the corrosion of 6061 Al-15%$_{(v)}$ SiC$_{(P)}$.

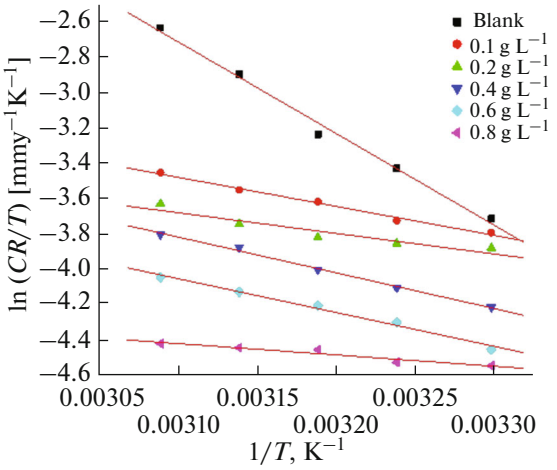

Fig. 6. Plots of ln(CR/T) vs ($1/T$) in 0.25 M hydrochloric acid containing different concentrations of starch for the corrosion of 6061 Al-15%$_{(v)}$ SiC$_{(P)}$.

Energy of activation (E_a) values of the inhibited solutions is lesser when compared with that of uninhibited solution. This decrease in the E_a value of the inhibited solution is suggestive of chemical adsorption of the starch inhibitor on the surface of the metal with a resultant closer approach to equilibrium during the experiment at higher temperatures. The adsorbed molecule on the metal surface blocks the process of charge transfer during the corrosion of Al-composite, this leads to the decrease in energy of activation. In the other words, the inhibitor molecule gets chemically adsorbed on the metal surface and reduces the electrochemical corrosion process [22]. The positive signs of ΔH_a reflects the endothermic process of Al-composite metal dissolution process. The entropy of activation (ΔS_a) values are negative which indicates that, in rate determining step the activated complex is association not dissociation i.e., decrease in the disorderness on going from reactants towards the activated complex [23].

Adsorption consideration: The mechanism of inhibition of corrosion by the addition of starch can be understood by studying the adsorption behavior of inhibitor molecule on 6061 Al-15%$_{(v)}$ SiC$_{(P)}$ composite metal surface. Information regarding how the inhibitor molecule interacted with aluminum composite surface can be obtained by adsorption isotherm. (θ) Degree of surface coverage values for different concentration was obtained from Potentiodynamic polarization studies and it was applied to various adsorption isotherms such as Langmuir, Freundlich, Temkin and Frumkin. The data was best fitted with Langmuir adsorption isotherm which can be related by the relationship (9) [24].

$$\frac{C}{\theta} = \frac{1}{K} + C, \qquad (9)$$

where, K is adsorption/desorption equilibrium constant (L mol^{-1}), C is the concentration of inhibitor molecule in the electrolyte, then θ is given by the Eq. (10)

$$\theta = \frac{I.E(\%)}{100}. \qquad (10)$$

The plot of $\frac{C}{\theta}$ verses C gave straight line; from the intercept $\frac{1}{K}$ values were obtained. Figure 7 indicates Langmuir adsorption isotherm plot for aluminum composite material.

The deviation from the unity value in the adsorption isotherm slope may due to the interaction between the adsorbed inhibitor molecule and Al-composite metal surface. The assumption of Langmuir adsorption isotherm is, adsorbed inhibitor molecule will not interact with each other; but this assumption not obeys in case of organic substances containing

Table 4. Activation parameters for different concentrations of starch in hydrochloric acid for the corrosion of 6061 Al-15%$_{(V)}$ SiC$_{(P)}$.

[Starch], g L^{-1}	E_a, kJ mol^{-1}	ΔH_a, kJ mol^{-1}	ΔS_a, J mol^{-1} K^{-1}
Blank	42.67	42.85	−184.28
0.1	15.68	13.57	−195.96
0.2	16.55	16.70	−197.63
0.4	20.30	19.63	−195.13
0.6	16.78	15.83	−195.69
0.8	7.72	5.29	−199.99

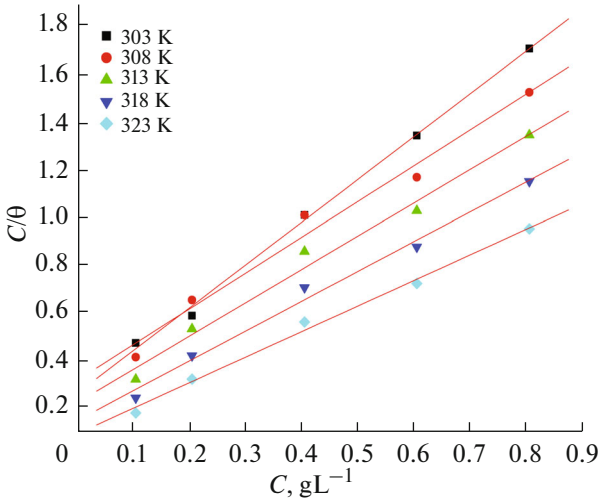

Fig. 7. Langmuir adsorption isotherm in 0.25M HCl containing different concentration of starch for 6061 Al-15%$_{(v)}$ SiC$_{(P)}$ composite.

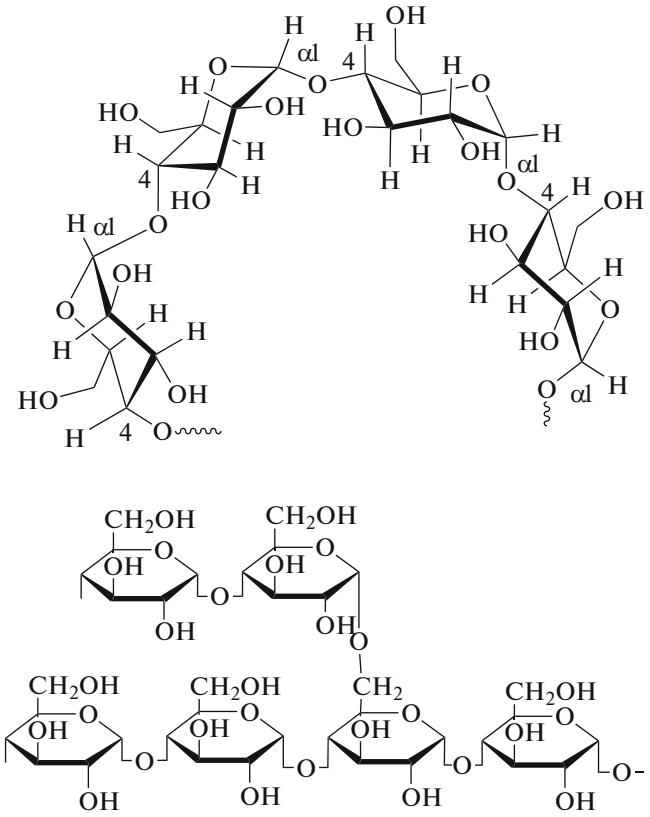

Fig. 8. (a) Amylose structure, (b) Amylopectin structure.

polar groups, which blocks anodic and cathodic sites of metal surface. The standard free energy of adsorption $\left(\Delta G^0_{\text{ads}}\right)$ is related to adsorption/desorption constant (K) by the following Eq. (11),

$$K = \frac{1}{C_{\text{water}}} \exp\left(\Delta G^0_{\text{ads}} / RT\right), \qquad (11)$$

where R is universal gas constant, T is the absolute temperature; as the concentration of water has unit g L^{-1} and K has unit L g^{-1} the value will become approximately 1000 [25].

Standard enthalpy of adsorption $\left(\Delta H^0_{\text{ads}}\right)$ and Standard entropy of adsorption $\left(\Delta S^0_{\text{ads}}\right)$ values were obtained by plotting ΔG^0_{ads} verses T. This gives linear plot; from the slope ΔS^0_{ads} value and from the intercept ΔH^0_{ads} values were calculated by using Gibbs Helmholtz Eq. (12).

$$\Delta G^0_{\text{ads}} = \Delta H^0_{\text{ads}} - T\Delta S^0_{\text{ads}}. \qquad (12)$$

According to Bentiss F et al, if ΔG^0_{ads} value is up to −20 kJ mol^{-1} then it is considered that there is an electrostatic interaction between the protonated inhibitor species and negatively charged metal surface i.e. physisorption. More negative value than −40 kJ mol^{-1} indicates sharing or transfer electrons from the inhibitor molecule to the surface of the metal through coordinate bond formation i.e. chemisorption [26]. Here, the negative value implies feasibility in corrosion process and the spontaneous adsorption of the inhibitor molecule on the metal surface. The ΔG^0_{ads} value is less than −20 kJ mol^{-1} and its value increased with increase in the temperature, this indicates the adsorption of the inhibitor molecule on 6061 Al-15%$_{(v)}$ SiC$_{(P)}$ composite is predominantly chemical adsorption [27].

If ΔH^0_{ads} value less than −40 kJ mol^{-1} then it correspond to physical adsorption, if it is approaching 100 kJ mol^{-1}, then it is considered as chemical adsorption. If ΔH^0_{ads} value less than −40 kJ mol^{-1} then it is considered as undergoing physical adsorption, if it is positive then it is considered as chemical adsorption. In this case ΔH^0_{ads} value is positive i.e. ΔH^0_{ads} = 46 kJ mol^{-1}, this indicates the chemical adsorption of inhibitor molecule over the surface of the Al-composite metal. The negative value of ΔS^0_{ads} is due to decrease in the disorderness of adsorbed inhibitor species.

MECHANISM OF CORROSION

Anodic dissolution reaction: In HCl medium, the protective layer of aluminum gets destroyed and corrosion attack takes place. Due to more negative potential of aluminum in galvanic series (E = −1.66 V Vs SCE) following reaction takes place (Eq. (13)),

$$\text{Al} \rightarrow \text{Al}^{3+} + 2\text{e}^-. \qquad (13)$$

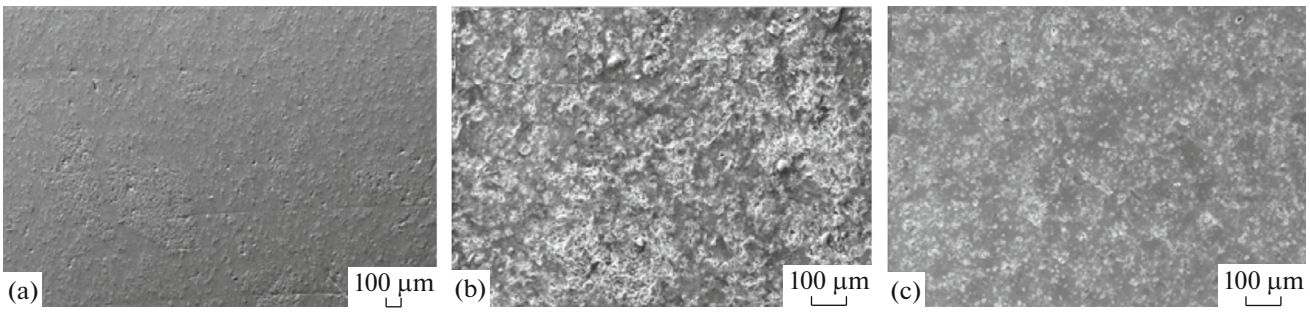

Fig. 9. SEM image of 6061 Al-15% vol SiC(P)material of a—freshly polished surface, b—immersed in 0.25 M HCl, c—immersed in 0.25 M HCl + 0.8 g L^{-1} starch at 303 K.

The chloride ions enhances the rate of metal dissolution, as they are chemically bonded in the interface it leads to the formation of mixture of oxohydroxo and chloro complexes of different forms given below [28]

$$\mathrm{Al}\left[\mathrm{O}_x(\mathrm{OH})_y(\mathrm{H_2O})_z\right] + \mathrm{Cl}^- \rightarrow \mathrm{Al}\left[\mathrm{O}_x(\mathrm{OH})_{y-1}\mathrm{Cl}(\mathrm{H_2O})_z\right] + \mathrm{OH}^-, \quad (14)$$

$$(\mathrm{AlOOH})_4 \cdot \mathrm{H_2O} + \mathrm{Cl}^- \rightarrow (\mathrm{AlOOH})_3 \cdot \mathrm{AlOCl} \cdot \mathrm{H_2O} + \mathrm{OH}^- \quad (15)$$

$$\mathrm{AlOOH} + \mathrm{Cl}^- \rightarrow \mathrm{AlOCl} + \mathrm{OH}^-, \quad (16)$$

$$\mathrm{Al(OH)_3} + \mathrm{Cl}^- \rightarrow \mathrm{Al\,(OH)_2\,Cl} + \mathrm{OH}^-. \quad (17)$$

Then, $[Al(Cl)_6]^{3-}$ is formed. Starch inhibitors containing plenty of –OH groups (shown in Fig. 13) get interacts with metal and protects the metal from undergoing corrosion.

$$\left[\mathrm{Al(Cl)_6}\right]^{3-}_{\mathrm{ads}} + [\mathrm{Starch}]^+ \rightarrow [\mathrm{AlCl_6}]^{3-}[\mathrm{Starch}]^+ \leftrightarrows \left[\mathrm{AlStarch}\right]^{3+}_{\mathrm{ads}} + \mathrm{Cl}_6^-. \quad (18)$$

Hydrogen evolution reaction: General cathodic reduction reaction in acidic environment is given below,

$$\mathrm{Al_2O_3} + \mathrm{H_3O}^+ + \mathrm{e}^- \leftrightarrows \mathrm{Al_2O_3\,(H_2O)} + 1/2\,\mathrm{H_2}. \quad (19)$$

The large polymer starch competes with protons and occupy cathodic region, forming Al-starch (Eq. (20)). The proton size is negligible compared to large molecular weight compound polymer starch. Therefore Starch as it is larger molecule; it covers almost all the parts of the metal and brings down both cathodic and anodic reactions under control.

$$\mathrm{Al} + [\mathrm{Starch}] + \mathrm{e}^- \leftrightarrows [\mathrm{Al\text{-}starch}]_{\mathrm{ads}}. \quad (20)$$

The presence of π-electrons and lone pair of electrons on oxygen atom are involved in protecting Al surface undergoing corrosion. The electrons are donated to the vacant *p*-orbitals of Al which leads to the formation of coordination bond between the metal surface and inhibitor molecule, as the metal get protected by forming coordination bond with inhibitor molecule, it can be suggest the chemical adsorption of the inhibitor molecule.

SURFACE STUDIES

SEM and elemental analysis: SEM image of freshly polished aluminum composite surface is shown in the Fig. 9a. The SEM image of aluminum composite is rough because of the presence of reinforcing SiC particulates and along with few scratches which occurred due to polishing. Due to the reinforcement, surface will become more heterogeneous and rough.

SEM image of aluminum composite in contact with 0.25 M hydrochloric acid is shown in the Fig. 9b. Figure 9b shows cavities because of the removal of SiC particulates from 6061 Al-15%$_{(v)}$ SiC$_{(p)}$ composite in contact with acid medium. This is because of the corrosion that occurs at the interface of SiC particles and aluminum matrix due to galvanic action in which SiC acts as cathodic to aluminum matrix and results in the detachment of SiC particulates from the aluminum matrix. Detachment of SiC particulates result in the formation of permanent cavities on the surface of composite material.

Figure 9c shows the smooth surface of 6061Al-15%$_{(v)}$SiC$_{(P)}$ immersed in 0.25 M hydrochloric acid medium containing starch inhibitor. After the addition of starch inhibitor surface of the aluminum composite became smoother, this is because; the zones of the

Table 5. Thermodynamic parameters for the adsorption of Starch in hydrochloric acid at different temperatures on 6061 Al-15%$_{(V)}$ SiC$_{(P)}$

Temp., K	$\Delta G^0_{\mathrm{ads}}$, kJ mol^{-1}	$\Delta H^0_{\mathrm{ads}}$, kJ mol^{-1}	$\Delta S^0_{\mathrm{ads}}$, J $\mathrm{mol}^{-1}\mathrm{K}^{-1}$
303	–20.70	46.00	218
308	–20.58		
313	–21.81		
318	–23.22		
323	–24.83		

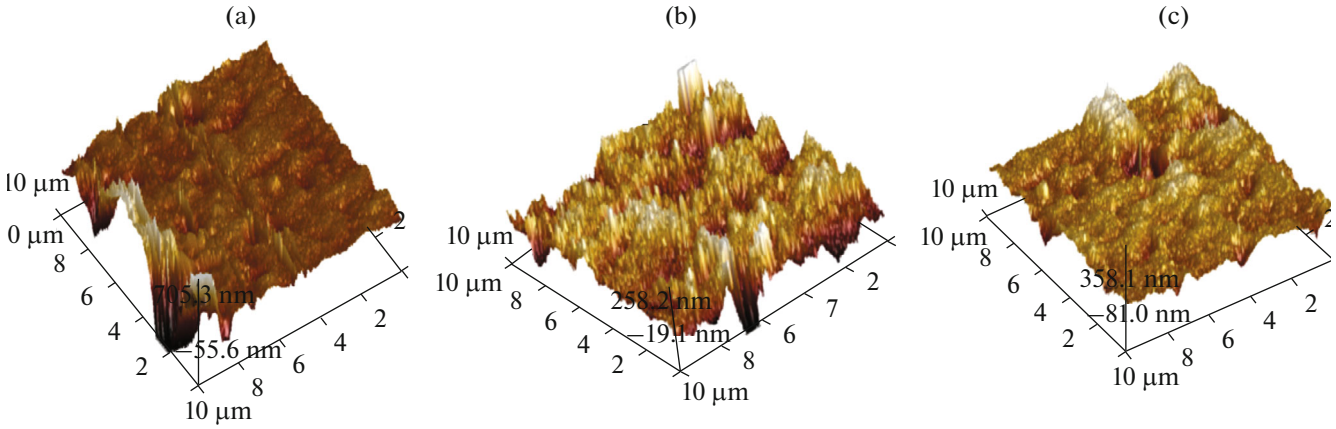

Fig. 10. 3D image of 6061 Al-15% vol SiC(P)material of a—freshly polished surface, b—immersed in 0.25 M HCl, c—immersed in 0.25 M HCl + 0.8 g L^{-1} starch at 303 K.

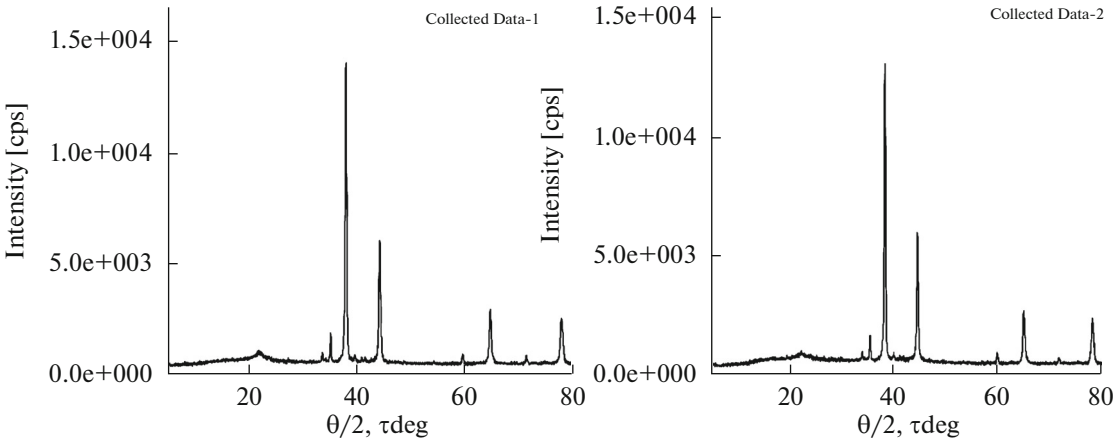

Fig. 11. a—XRD spectrum for corroded 6061 Al-15% $_{(v)}$ $SiC_{(P)}$ composite. b—XRD spectrum for 6061 Al-15% $_{(v)}$ $SiC_{(P)}$ composite immersed in inhibited solution.

detached SiC particulates were blocked by the starch inhibitor and get adsorbed onto the metal surface thus creating the protective barrier between metal surface and the medium.

EDX spectrum corresponds to un-corroded, corroded and inhibited samples were analyzed. The data of elemental mapping is given in the Table 6.

Increase in % composition of oxygen and chlorine in the corroded sample is indicative of dissolution of stable oxide film layer. Peak due to carbon in the inhibited sample confirms the adsorption of starch on the surface of the material.

AFM analysis. The 3-dimensional (3D) images of 6061 Al-composite is given in the Fig. 10. Figure 10a–10c corresponds to freshly polished metal surface image, specimen immersed in 0.25 M HCl medium and specimen + 0.25 M HCl + 0.8 g L^{-1} starch respectively. The average surface roughness (R_a), Root mean square (RMS) roughness (R_q) and peak-valley maximum (P–V) values were given in the Table 7. It is evident from the Table 7, that R_a, R_q and (P–V) values of inhibited sample is very less compared to polished and uninhibited sample this indicates the binding of the inhibitor molecule over the metal surface.

XRD analysis. XRD spectrums for the corroded powdered 6061 Al-15% vol SiC(P)sample and for the

Table 6. EDX data for 6061 Al-15% $_{(v)}$ $SiC_{(P)}$ composite surface analysis

Samples	(%) Composition				
	Al	Si	O	Cl	C
Freshly polished 6061 Al-15% $_{(v)}$ $SiC_{(P)}$	79.19	13.88	6.93	–	24.48
Specimen immersed in 0.25 M HCl medium	43.08	4.96	22.67	0.19	16.72
Specimen + 0.25 M HCl + 0.8 g L^{-1} starch	54.18	10.65	10.68	–	24.64

Table 7. AFM data obtained for 6061 Al-15% $_{(v)}$ SiC$_{(P)}$ composite surface analysis

Samples	R_a, nm	R_q, nm	(P–V), nm
Freshly polished 6061 Al-15% $_{(v)}$ SiC$_{(P)}$ material	38.3	50.8	498
Specimen immersed in 0.25 M HCl medium	50.7	65.7	547
Specimen + 0.25 M HCl + 0.8 g L^{-1} starch	28.4	36.5	331

sample with inhibitor were given in the Fig. 11a, 11b respectively. The Fig. 11a showed more intense peak i.e. 147.54, 265.55, 986.52, 9760.95, 196.46, 3926.88, 399.15, 1901.55, 308.32, and 1488.2; Fig. 11b showed less intense peak i.e. 142.32, 250.26, 834.92, 9099.05, 144.93, 3872.56, 1801.16, 306.16 and 1413.65. This decrease in the peak intensity for the sample with inhibitor is due to the binding of the starch molecule onto the surface of the metal.

CONCLUSION

Based upon the studies carried out following conclusions are drawn,

• Starch emerged as an effective ecofriendly, green inhibitor for the corrosion control of aluminum composite material

• Inhibition efficiency of starch increased with increase in the concentration of starch and as well as temperature.

• Kinetic and thermodynamic studies revealed the chemical adsorption of the inhibitor and it obeyed Langmuir adsorption isotherm.

• The adsorption of starch molecule onto the surface of the metal was supported by surface studies like SEM, EDAX, AFM and XRD analysis.

• Results obtained by potentiodynamic polarization method and electrochemical impedance method were in good agreement with one another.

ACKNOWLEDGMENTS

Ms. Charitha B. P. is very thankful to Manipal University for Research Fellowship and Chemistry Department of M.I.T. Manipal for laboratory facilities.

REFERENCES

1. Bobic, B., Mitrovic, S., Babic, M., and Bobic, I., in *Corrosion of Metal-Matrix Composites with Aluminium Alloy Substrate,* New York: McGraw-Hill, 2010, vol. 32, pp. 3–11.
2. Monticelli, C., Zucchi, F., Brunoro, G., and Trabanelli, G., *J. Appl. Electrochem.,* 1997, vol. 27, pp. 325–334.
3. *Biopolymers: Making Materials Nature's Way*, Background Paper, OTA-BP-E-102, U.S. Congress, Office of Technology Assessment, Washington: Government Printing Office, 1993.
4. Deepa Prabhu and Padmalatha Rao, *J. Environ. Chem. Eng.,* 2013, vol. 1, pp. 676–683.
5. Deepa Prabhu and Padmalatha Rao, *Int. J. ChemTech Res.,* 2013, vol. 5, pp. 2690–2705.
6. Deepa Prabhu and Padmalatha Rao, *Int. J. Corros.,* 2013, vol. 2013, pp. 1–11.
7. Stupnise K-Lisac, E., Gazivoda, A., and Madza Rac, M., *Electrochim. Acta,* 2002, vol. 47, pp. 4189–4194.
8. Shahin, M., Bilgic, S., and Yilmaz, H., *Appl. Surf. Sci.,* 2003, vol. 195, pp. 1–7.
9. Li, W., He, Q., Zhang, S., Pei, C., and Hou, B., *J. Appl. Electrochem.,* 2008, vol. 37, pp. 289–295.
10. Fontana, M.G., *Corrosion Engineering,* Singapore: McGraw-Hill, 1987, vol. 3.
11. Lenderink, H.J.W., Linden, M.V.D., and De Wit, J.H.W., *Electrochim. Acta,* 1993, vol.38, pp. 1989–1992.
12. De Wit, J.H.W. and Lenderink, H.J.W., *Electrochim. Acta,* 1996, vol. 41, pp. 1111–1119.
13. Ehteram Noor, A., *Mater. Chem. Phys.,* 2009, vol. 114, pp. 533–541.
14. Frers, S.E., Stefenel, M.M., Mayer, C., and Chierchie, T., *J. Appl. Electrochem.*, 1990, vol. 20, pp. 996–999.
15. Mansfeld, F., Lin, S., Kim, K., and Shih, H., *Corros. Sci.,* 1987, vol. 27, pp. 997–1000.
16. Mansfeld, F., Lin, S., Kim, K., and Shih, H., *Werkst. Korros.,* 1988, vol. 39, p. 487.
17. Sanat Kumar, B. S., Nayak, J. and Shetty, A.N., *J. Coat. Technol. Res.,* 2011, vol. 4, pp. 483–493.
18. Bessone, J.B., Salinas, D.R., Mayer, C., Ebert, M., and Lorenz, W.J., *Electrochim. Acta,* 1992, vol. 37, pp. 2283–2290.
19. Yahalom, J., *Corros. Sci.,* 1972, vol. 12, pp. 867–868.
20. Ameer, M.A., Khamis, E., and Al-Senani, G., *J. Appl. Electrochem.,* 2002, vol. 32, pp. 149–156.
21. Oguzie, E.E., Njoku, V.O., Enenebeaku, C.K., Akalezi, C.O., and Obi, C., *Corros. Sci.,* 2008, vol. 50, pp. 3480–3486.
22. Ashassi-Sorkhabi, H., Shaabani, B., and Seifzadeh, D., *Appl. Surf. Sci.,* 2005, vol. 239, pp. 154–164.
23. Bouklah, M., Hammouti, B., Lagrenee, M., and Bentiss, F., *Corros. Sci.,* 2006, vol. 48, pp. 2831–2842.
24. Soltani, N., Behpour, M., Ghoreishi, S.M., and Naeimi, H., *Corros. Sci.,* 2010, vol. 52, pp. 1351–1361.
25. Xianghong, Li. and Shuduan, Deng., *Corros. Sci.,* 2012, vol. 65, pp. 299–308.
26. Bentiss, F., Traisnel, M., and Lagrenee, M., *J. Appl. Electrochem.,* 2001, vol. 31, pp. 41–48.
27. Quraishi, M.A., Rawat, J., and Ajmal, M., *J. Appl. Electrochem.,* 2000, vol. 30, pp. 745–751.
28. Tomesanyi, L., Varga, K., Bartik, I., Horanyi, G., and Maleczki, E., *Electrochim. Acta,* 1989, vol. 34, pp. 855–859.